

RESEARCH

Open Access



# Fast $\ell_1$ -minimization algorithm for robust background subtraction

Huaxin Xiao<sup>\*</sup>, Yu Liu and Maojun Zhang

## Abstract

This paper proposes an approximative  $\ell_1$ -minimization algorithm with computationally efficient strategies to achieve real-time performance of sparse model-based background subtraction. We use the conventional solutions of the  $\ell_1$ -minimization as a pre-processing step and convert the iterative optimization into simple linear addition and multiplication operations. We then implement a novel background subtraction method that compares the distribution of sparse coefficients between the current frame and the background model. The background model is formulated as a linear and sparse combination of atoms in a pre-learned dictionary. The influence of dynamic background diminishes after the process of sparse projection, which enhances the robustness of the implementation. The results of qualitative and quantitative evaluations demonstrate the higher efficiency and effectiveness of the proposed approach compared with those of other competing methods.

**Keywords:** Approximative  $\ell_1$ -minimization, Background subtraction, Sparsity representation

## 1 Introduction

Foreground or motion detection is a problem involving the segmentation of moving objects from a given image sequence or video surveillance. Because of its fundamental and pivotal role in the field of advanced computer vision, such as tracking, event analytics, and behavior recognition, foreground segmentation has drawn considerable attention over the past decades [1]. Generally, background subtraction (BGS) is an effective and efficient technique for addressing the issue of foreground segmentation. In this technique, some strategies are employed to establish or estimate a background model, and then the current frame is compared with the background model to segment the foreground objects. However, the scene typically includes other periodical or irregular motion (e.g., shaking trees and flowing water) arising from the nature of the captured video, which challenges the feasibility of BGS [2].

Various methods have been proposed to deal with the BGS problem, such as the statistical models: Gaussian

mixture model (GMM) [3]. Frame-based methods consider spatial configurations as a significant cue for background modeling, such as eigen-background model [4]. In addition, a number of popular approaches have been developed that are not restricted to the above categories, such as artificial neural networks like self-organizing background subtraction (SOBS) [5] and local feature descriptors [2]. All of the abovementioned approaches and algorithms can be categorized as classic BGS methods that make overly restrictive assumptions on the background model.

In this paper, we propose a sparse-based BGS strategy that can be distinguished from the above classic methods owing to looser model assumptions. We employ a dictionary learning algorithm to train bases, which formulates the background modeling step as a sparse representation problem. The current image frame is then projected over this trained dictionary to obtain a corresponding coefficient. Different scene contents have different coefficients, reflecting the fact that the foreground does not lie on the same bases or subspaces spanned by the background. This condition is helpful in identifying changes in the scene by comparing the spanned coefficients. Given that dynamic texture and statistical noise are typically distributed through the entire space anisotropically, their influence on an actual signal will be obviously weakened

<sup>\*</sup>Correspondence: huaxinxiao@hotmail.com  
College of Information Systems and Management, National University of Defense Technology, Sanyl Road, 410073 Changsha, China

after application of the sparse projection process. This characteristic enhances the robustness of the proposed method to corrupted signals and noisy scenes.

On the other hand, existing  $\ell_1$ -minimization ( $\ell_1$ -min) or sparse coding algorithms are not sufficiently fast for real-time implementation of BGS. Inspired by the theory of data separation of sparse representations [6], we simplify the  $\ell_1$ -min process and apply it as a pre-processing step. In the proposed approximative  $\ell_1$ -min algorithm, the test/observed signal is separated into a number of basic atoms. For each atom, the sparse coefficient is calculated by an existing  $\ell_1$ -min algorithm, which obtains a number of sparse coefficient vectors equivalent to the total number of atoms. The sparse coefficient of the atom is defined as the children sparse vector in this paper. We assume that any observed/test data can be linearly represented by these atoms. Consequently, the sparse coefficient of any test/observed signal can also be regarded as a linear combination of the children sparse vectors. Therefore, the  $\ell_1$ -min process is simplified into addition and multiplication operations.

Compared with the existing sparse-based [7–10] methods (reviewed in Section 2.2), the main contributions of the proposed method can be summarized as follows.

1. A novel formulation of BGS is proposed. The proposed method regards the distribution of sparse coefficients rather than the sparse error as the criterion of foreground detection, where the existing sparse-based BGS directly utilizes the frames of scenes [8, 9] or learned frames [10] to construct the dictionary. A two-stage sparse projection processing is employed to obtain precise detection results even with dynamic scenes.
2. A novel  $\ell_1$ -min algorithm is proposed for real-time BGS implementation. The existing  $\ell_1$ -min algorithms are computationally expensive for the proposed BGS framework. We therefore convert the iterative processing of an existing  $\ell_1$ -min algorithm into simple addition and multiplication operations, with minimal sacrifice to the accuracy.

## 2 Related work

### 2.1 $\ell_1$ -min algorithms

For a given signal  $\mathbf{y} \in \mathbb{R}^m$ , the sparse model is a process of pursuing the sparsest solution  $\boldsymbol{\alpha} \in \mathbb{R}^n$  of  $\mathbf{y}$  over a pre-learned dictionary  $\mathbf{D} \in \mathbb{R}^{m \times n}$  as follows:

$$P_\lambda : \hat{\boldsymbol{\alpha}} = \arg \min_{\boldsymbol{\alpha}} \left( \lambda \|\boldsymbol{\alpha}\|_1 + \frac{1}{2} \|\mathbf{y} - \mathbf{D}\boldsymbol{\alpha}\|_2^2 \right). \quad (1)$$

where  $\|\boldsymbol{\alpha}\|_1$  represents the sparse constraint and  $\lambda$  is a scalar weight.

In [11],  $P_\lambda$  was regarded as a LASSO problem and solved by least angle regression [12]. Numerous methods have

been subsequently proposed to solve the unconstrained problem  $P_\lambda$ , such as the coordinate-wise descent method [13], fixed-point method [14], and Bregman iterative algorithm [15]. Presently,  $\ell_1$ -min algorithms for sparse model or CS have achieved remarkable breakthroughs with respect to recovered results and computational efficiency. However, these algorithms are not sufficiently fast for real-time implementation of BGS because optimization is conducted in an iterative manner. Hence, the motivation of the present study is the development of a specialized  $\ell_1$ -min algorithm for real-time sparse-based BGS.

### 2.2 Sparse-based BGS

Sparse-based BGS avoids modeling of the background with parametric or non-parametric models, which provides a substantial advantage. The only assumption made on the background is that any variation in its appearance can be captured by the sparse error. Cevher et al. [7] regarded BGS as a sparse approximation problem and obtained a low-dimensional compressed representation of the background. Huang et al. [8] added a prior of group sparsity clustering as a new constraint in the process of sparse recovery and extended CS theory to manage dynamic background scenes efficiently. However, the balance between the signal sparsity prior and group sparsity prior required control by parametric tuning. Sivalingam et al. [9] regarded the foreground as the  $\ell_1$ -min of the difference between the current frame and the estimated background model. Zhao et al. [10] proposed a robust dictionary learning algorithm that prunes the foreground objects out as outliers at the training step. Xue et al. [16] cast foreground detection as a fused Lasso problem with a fused sparsity constraint. Later, Xiao et al. [17] extended the assumptions of CS for BGS [7] by adding an assumption that the projection of the noise over the dictionary is irregular and random.

### 2.3 Low rank-based BGS

The low-rank model based BGS assumes that the background of a scene can be captured by a low-rank matrix while the foreground can be regarded as a sparse error [18]. Qiu and Vaswani [19] proposed a real-time principal components pursuit (PCP) algorithm to recover the low matrix. Subsequently, robust PCA (RPCA) [20] was proposed to pursue the low-rank representation by an iterative optimization approach. Cui et al. [21] utilized low-rank decomposition to obtain the background motion and group sparsity [8] by which the foreground was constrained. The DECOLOR [22] method incorporates the Markov random field prior to restrict the foreground model and domain transformations to address a moving background. A simple and fast incremental PCP (incPCP) [23] is proposed for video background modeling. In a most recent work [24],

the authors estimated a dense motion field to facilitate the process of matrix restoration.

Subspace tracking also plays an important role in low rank-based BGS. He et al. [25] proposed an online subspace estimation algorithm GRASTA to separate the foreground and background in sub-sampled video. Seidel et al. [26] replaced the  $\ell_1$ -norm in RPCA with a smoothed  $\ell_p$ -norm and presented a robust online subspace tracking algorithm based on alternating minimization on manifolds. Xu et al. [27] formulated the online estimation procedure as an approximate optimization process on a Grassmannian.

### 3 Proposed method

#### 3.1 Proposed approximative $\ell_1$ -min algorithm

This section will introduce the proposed approximative  $\ell_1$ -min algorithm. Before describing the details, we use an example in Fig. 1 to express the core intuition of the algorithm. As shown in the left part, the sparse solutions of the basis vectors  $\mathbf{e}_m$  are defined as the children sparse vectors  $\beta_m$  which will be employed to accelerate the proposed algorithm. For an input, it can also be separated into the similar patterns which have a linear relation  $\gamma$  with the base patterns. The sparse solution of the input is boiled down to the linear combination of the children sparse vectors. The iterative process in conventional  $\ell_1$ -min algorithms is simplified to linear operation.

Similarly, a given signal  $\mathbf{y} \in \mathbb{R}^m$  can be separated as a linear combination of basis functions  $\mathbf{e}_i \in \mathbb{R}^m$  as follows:

$$\mathbf{y} = \gamma_1 \mathbf{e}_1 + \dots + \gamma_i \mathbf{e}_i + \dots + \gamma_m \mathbf{e}_m, \tag{2}$$

where  $\gamma_i$  is the projection of  $\mathbf{y}$  over  $\mathbf{e}_i$ . The selection of  $\mathbf{e}_i$  varies, and  $\mathbf{y}$  can be separated into a variety of base patterns. The only criterion of basis selection is the independency of each basis, i.e., the bases must span the entire

space of  $\mathbf{y}$ . In this paper, we employ the simplest type of  $\mathbf{e}_i$ , i.e., the identity basis vectors:

$$\mathbf{e}_i = \left[ 0, 0, \dots, 1, \dots, 0, 0 \right]^T, \tag{3}$$

where the projection  $\gamma_i$  of  $\mathbf{y}$  over  $\mathbf{e}_i$  is the pixel value of  $\mathbf{y}$  at site  $i$  in the problem of image or video processing.

Each  $\mathbf{e}_i$  can be regarded as the observed signal in the unconstrained problem  $P_\lambda$ , and we can therefore convert Eq. (1) as follows:

$$P_\lambda^e : \hat{\beta}_i = \arg \min_{\beta_i} \left( \lambda \|\beta_i\|_1 + \frac{1}{2} \|\mathbf{e}_i - D\beta_i\|_2^2 \right), \tag{4}$$

where  $\beta_i$  is the sparse coefficient of  $\mathbf{e}_i$  and is defined as the children sparse vector. In this paper, we solve the problem  $P_\lambda^e$  with the Bregman iterative algorithm [15]. For the same size signals, Eq. (4) only need to be solved one time.

It has been determined that most data can be classified as multi-modal data composed of irrelevant subcomponents, for example, imaging data obtained from neurobiology are typically composed of neuron soma, cones, and rod cells [6]. Besides [6], Donoho and Huo [28] have suggested that the selection of distinct bases that are adapted to different subcomponents will facilitate separation. Inspired by [6] and [28], we assume that the sparse solution  $\alpha$  of  $\mathbf{y}$  can be separated into a linear combination of its children sparse vectors  $\beta_i$  as follows:

$$\alpha \approx \gamma_1 \beta_1 + \dots + \gamma_i \beta_i + \dots + \gamma_m \beta_m. \tag{5}$$

For a given problem or application, once the size of the processing signal is decided,  $\mathbf{e}_i$  is also known. Then, we can pre-solve the children sparse vector  $\beta_i$  in Eq. (4) by an existing  $\ell_1$ -min algorithm. The sparse solution  $\alpha$  of a new signal  $\mathbf{y}$  can be rapidly estimated by Eq. (5) where the weights  $\gamma_i$  is the value of  $\mathbf{y}$  at site  $i$ . The iterative process in

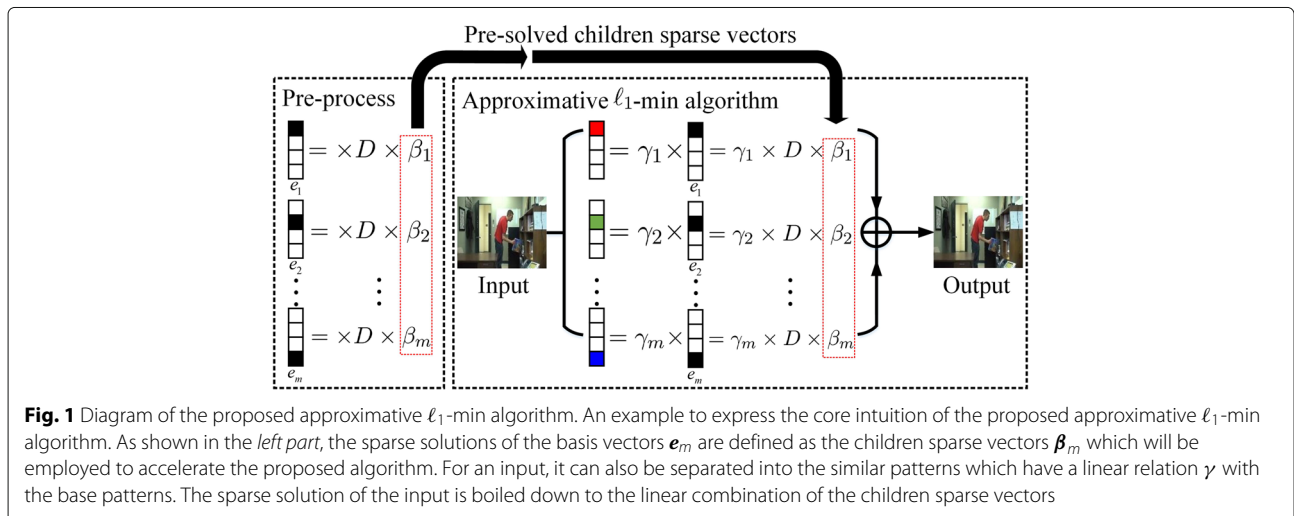


**Fig. 1** Diagram of the proposed approximative  $\ell_1$ -min algorithm. An example to express the core intuition of the proposed approximative  $\ell_1$ -min algorithm. As shown in the left part, the sparse solutions of the basis vectors  $\mathbf{e}_m$  are defined as the children sparse vectors  $\beta_m$  which will be employed to accelerate the proposed algorithm. For an input, it can also be separated into the similar patterns which have a linear relation  $\gamma$  with the base patterns. The sparse solution of the input is boiled down to the linear combination of the children sparse vectors

existing  $\ell_1$ -min algorithms is replaced by simple addition and multiplication operations.

An important question remains concerning the numerical distance between the sparse solution of an existing  $\ell_1$ -min algorithm and the proposed algorithm. The distance is, in fact, acceptable for many applications that demand a compositive result (e.g., foreground detection or recognition), but not for applications that expect the highest quality result possible (e.g., image deblurring or denoising). If tolerable in a specific application, the proposed  $\ell_1$ -min algorithm can be used as an acceleration engine, which can dramatically improve the computational efficiency. The numerical error between the solution of an existing  $\ell_1$ -min and the proposed algorithm and the computational burden will be discussed in detail in Section 4.1.

### 3.2 Proposed sparse-based BGS

This section provides details of the proposed BGS method, and an overview of the proposed method is shown in Fig. 2. For greater completion efficiency and accuracy, we first separate the input image sequence into small patches and then scale down the resolution. Similarly, the sub-sampled images are divided into the same number patches as the original resolution. The low-resolution frames are subsequently projected over a pre-learned dictionary with the proposed fast  $\ell_1$ -min algorithm. Rather than casting the foreground detection as a sparse error estimation problem [9], we employ a comparison between the background and foreground which based on the distribution of sparse coefficients.

According to the sparse coefficients, we can pick up the patches that contain the foreground object. The selected patches of sub-sampled images correspond the same position of the original frames. For eliminating the inaccurate results caused by image patches, a second-stage of patch refinement is applied to the region determined in the first stage to obtain the final foreground detection.

#### 3.2.1 Background model

The BGS problem is usually formulated as a linear combination of a background model  $\mathbf{I}_B$  and a foreground

candidate  $\mathbf{I}_F$ . In the existing sparse-based BGS [8–10], the background model is regarded as a linear combination of the dictionary while the dictionary is simple the combination of previous frames. However, this strategy is impractical for real-time implementation when image size becomes large. Therefore, in the present study, the original image sequence is first scaled-down with a 4:1 ratio. Then, each low-resolution frame  $\mathbf{I}'$  is detached into  $N$  non-overlapping patches  $\{P^i | i = 1, 2, \dots, N\}$  (see Fig. 2). For each patch  $P^i$ , the background model  $P_B^i$  can be formulated as follows:

$$P_B^i = \mathbf{D}\alpha_i, \tag{6}$$

where  $\alpha_i$  is the sparse coefficient and  $\mathbf{D}$  is a pre-learned and overcompleted dictionary.

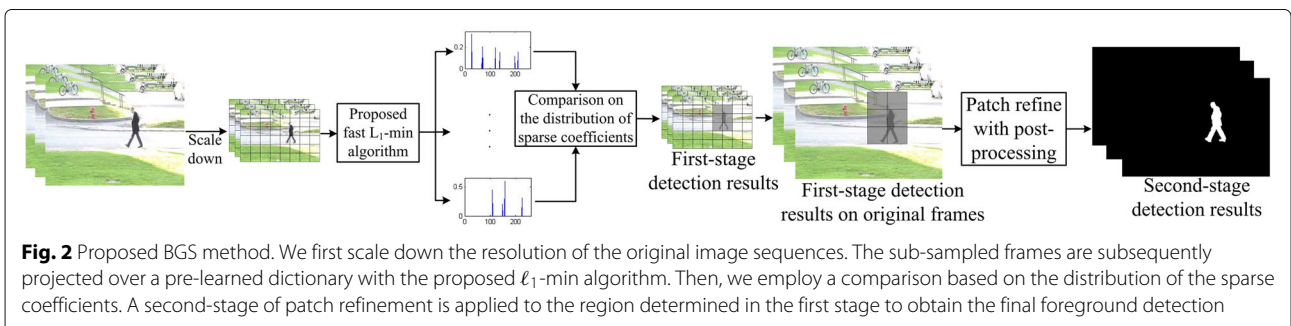
Compared with traditional methods of obtaining bases such as wavelet and PCA, overcompleted dictionary learning does not emphasize the orthogonality of bases. Thus, its representation of the signal has better adaptability and flexibility. In this paper, the dictionary  $\mathbf{D}$  is pre-learned by the algorithm in [29] with a natural image training set. This paper constructs the training set with some images that contains nature scenes. The images for foreground detection do not include dictionary training set. The training images are separated as the same size as the patches  $P^i$ . We set the regularization parameter in [29] as  $1.2/K$  where  $K \times K$  is the size of  $P^i$ . In this paper,  $\mathbf{D}$  is global and suitable for arbitrary scenes, which indicates that, once  $\mathbf{D}$  is learned, it can be employed for any testing dataset.

Before solving the sparse coefficients  $\alpha_i$ , we construct the image basis  $\mathbf{e}$  in Eq. (3) of the same size as  $P_i$  and obtain the children sparse vectors  $\beta$  of  $\mathbf{e}$ . Then, the background model  $P_B^i$  in Eq. (6) can be rewritten as follows:

$$P_B^i = \mathbf{D}\alpha_i \approx \mathbf{D} \times \sum_j \gamma_j^i \beta_j, \tag{7}$$

where  $\gamma_j^i$  are the projection coefficients of  $P_B^i$  over  $\mathbf{e}_j$ . For a patch  $P^i$  of the current frame  $\mathbf{I}'$ , the foreground patch  $P_F^i$  is formulated as follows:

$$P_F^i = P^i - P_B^i \approx P^i - \mathbf{D} \times \sum_j \gamma_j^i \beta_j. \tag{8}$$



Actually, no matter how precise  $P_B^i$  is, it cannot completely predict the state of the next frame. As such, a slight difference exists between the current frame patch  $P^i$  and the background model  $P_B^i$ , which can lead to false detection. To avoid differences caused by dynamic textures or signal noise, we project the current frame patch  $P^i$  over the pre-learned dictionary  $\mathbf{D}$  and compute the sparse coefficient  $\alpha'$ . Then, Eq. (8) is converted as follows:

$$\begin{aligned} P_F^i &= \mathbf{D}\alpha' - \mathbf{D}\alpha \approx \mathbf{D} \times \sum_j \gamma_j^i \beta_j - \mathbf{D} \times \sum_j \gamma_j^i \beta_j \\ &= \mathbf{D} \times \sum_j (\gamma_j^i - \gamma_j^i) \beta_j, \end{aligned} \quad (9)$$

where  $\gamma_j^i$  are the projection coefficients of the current frame patch  $P^i$  over the basis  $\mathbf{e}_j$ .

### 3.2.2 First-stage foreground detection

As described in Section 1, we apply the distribution of sparse coefficients rather than the sparse error to estimate the foreground. This is done because the appearance of the foreground in the scene will cause changes in the projection of  $P_B^i$  over  $\mathbf{D}$ . In other words, when a current frame containing moving objects is presented by the subspace spanned by pure background bases, the unchanged area of the scene can be recovered. In contrast, the changed area is reconstructed according to the deviation in the projection on the subspace. Measuring this deviation satisfies the purpose of foreground detection. In the first stage, or low-resolution stage, the region where a foreground may exist can be detected as follows:

$$\begin{cases} \Delta_1(i) = \frac{\|\sum_j \gamma_j^i \beta_j - \sum_j \gamma_j^i \beta_j\|_1}{\|\sum_j \gamma_j^i \beta_j\|_1}, \\ \Delta_2(i) = \frac{\|\sum_j \gamma_j^i \beta_j\|_0 - \|\sum_j \gamma_j^i \beta_j\|_0}{\|\sum_j \gamma_j^i \beta_j\|_0}, \end{cases} \quad (10)$$

where  $i$  represents the  $i$ th patch of  $\mathbf{I}'$  and  $\Delta_1(i)$  and  $\Delta_2(i)$  are the differences in the distributions and values of the sparse coefficients between the current patch  $\mathbf{D}\alpha'$  and the background model  $\mathbf{D}\alpha$  in Eq. (9). Due to adoption of identity basis vectors as basis functions  $\mathbf{e}_j$ ,  $\gamma_j^i$  equals to the pixel value of the  $i$ th patch at site  $j$ .

Given that the distributions and values of the sparse coefficients reflect which subspace is expanded by the test frame, we can use these parameters to determine whether a monitored scene has moving content. Specifically, an unchanging image content tends to have identical distributions and corresponding values. In contrast, if a foreground object enters the scene and changes the content, it generates distinct distributions and values for the sparse coefficients.

To facilitate the detection operation, we combine  $\Delta_1(i)$  and  $\Delta_2(i)$  as follows:

$$\Delta(i) = \mu_1 \Delta_1(i) + \mu_2 \Delta_2(i), \quad (11)$$

where  $\mu_1$  and  $\mu_2$  are the unitary parameters that determine the respective weights of  $\Delta_1(i)$  and  $\Delta_2(i)$ . Because the  $\ell_1$ -norm, or least absolute deviation, can better represent the distribution of the sparse coefficient and ensure a more distinguishable difference,  $\mu_1$  is set to a relatively large value (0.60–0.75) as the dominant weight, while  $\mu_2$  is smaller (0.25–0.40).

The first-stage detection results in the original resolution by different criteria are shown in Fig. 3. We employ  $\Delta_1$  and  $\Delta_2$ , respectively, to segment the foreground which are shown in Fig. 3c, d. We can find that the results by  $\Delta_1$  are more accurate. However, some foreground patches (the book in the first row) are missed by  $\Delta_1$ . Though the results by  $\Delta_2$  have more false-positive pixels, they can still complement the detection results by  $\Delta_1$ . Therefore, we combine  $\Delta_1$  and  $\Delta_2$  in Eq. (11) to obtain a better result as shown in Fig. 3e. However, the results by Eq. (11) are still rough and inaccurate. A second-stage refinement should be performed.

### 3.2.3 Second-stage foreground detection

We denote the foreground patches detected by the first-stage in original frame  $\mathbf{I}$  as  $\{P_t^F \in \mathbb{R}^{K \times K} | t = 1, 2, \dots, n\}$ . For each patch  $P_t^F$  shown by the green squares in Fig. 4, we use a smaller  $L \times L$  sliding window shown by the blue square on the right-hand side of Fig. 4 to determine whether the central pixel in red belongs to the foreground. Similar to the process employed in the first stage, we train a new dictionary  $\mathbf{D}'$  whose atoms have the dimension  $L^2$ . Equations (9–11) are again employed, and the difference values  $\Delta$  in Eq. (11) are obtained for each  $L \times L$  patch. To acquire a more precise result, we further process  $\Delta$  as follows:

$$\Delta' = \Delta + \sum_{k \in \text{neighbor}(\Delta)} \Delta(k), \quad (12)$$

where  $\text{neighbor}(\Delta)$  defines a neighborhood patch of the current sliding window, as shown by the black square on the right-hand side of Fig. 4.

Equation (12) enhances the effect of segmentation because the question of whether a pixel belongs to a foreground object depends not only on its own intensity but also on the intensities of its neighborhood regions. As shown in Fig. 3d, patch-wise refinement based on first-stage detection achieves far more precise results, where the resulting foreground outlines show good agreement with the ground truth results shown in Fig. 3b.

### 3.2.4 Background update

An important characteristic for any BGS algorithm is to continuously update the learned model over time. The update process affords the ability to accommodate gradually changing illumination conditions and adapt to new objects that appear in a scene. Because the dictionary used

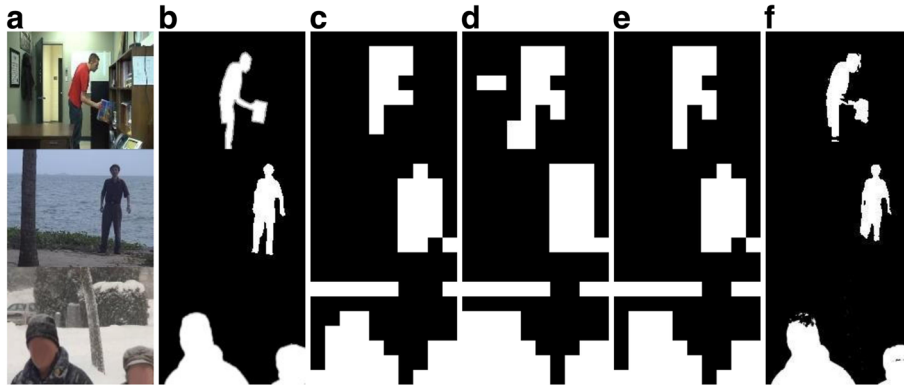


**Fig. 3** Two-stage foreground detection. **a** Frames extracted from the Office [38], Water surface [30], and Skating [38] datasets. **b** Ground truth. **c** First-stage detection results by  $\Delta_1$ . **d** First-stage detection results by  $\Delta_2$ . **e** First-stage detection results by  $\Delta$ . **f** Second-stage detection results by proposed BGS method

in our work is learned as a pre-processing step employing arbitrary images, the update process of background  $P_B^i$  requires updating the sparse coefficients  $\alpha_i$  of the background model every frame or after some number of frames according to the implementation requirements. The updating strategy of the background model is given as follows:

$$\alpha_{i+1} = (1 - \rho)\alpha_i + \rho\alpha'_i, \tag{13}$$

where  $\alpha_i$  and  $\alpha'_i$  are the sparse coefficients of background model  $P_B^i$  and current image patch  $P^i$ , respectively, and  $\rho \in [0.2, 0.5]$  is the learning rate.

In the proposed method, we initialize the background model with the first several frames and update only the sparse coefficients of the image patches that are distinguished as background. In other words, if the  $i$ th image patch  $P^i$  belongs to the foreground, the proposed method does not update the corresponding sparse coefficient  $\alpha_i$  of the background model. We evaluate the performance of the background update. The dataset Airport [30] with a stationary person is selected. As shown in Fig. 5a, a

person remains stationary. The initialization data of Airport which is free from foreground objects is not available. The updated background images are shown in Fig. 5b. When an object remains stationary, the proposed method will regard it as a background as shown the first two rows of Fig. 5. When the object starts to move again, it will be formulated as a foreground as shown in the last row of Fig. 5. Benefiting from the power of sparse representation, the simple update rule in Eq. (13) can obtain a proper background model for foreground detection. This is because that sparse coefficients are more robust and effective than the pixel intensity. The overall BGS method is described in Algorithm 1.

#### 4 Experimental results and discussion

To evaluate the performance of the proposed method, the experimental study was divided into two parts: one part tested the proposed approximate  $\ell_1$ -min algorithm and the other part tested the proposed BGS method. All experiments are performed using MATLAB on a laptop with a 2.50-GHz Intel Core i7-4710MQ processor and 16 GB of memory.

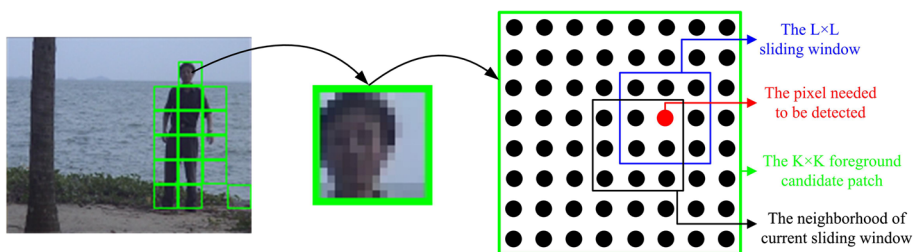


**Fig. 4** Sliding window processing of second-stage detection. The *left image* contains the first-stage detection result, where the foreground regions are outlined by *green squares*. The *right-hand image* is a representation of the sliding window process for a single foreground region. The *black dots* in the *green square region* represent  $K \times K$  foreground candidate pixels, whereas the *red dot* denotes the pixel selected for foreground detection. The size of the sliding window is  $L \times L$ , as shown by the *blue square*. The *black square* represents a neighborhood patch of the current sliding window

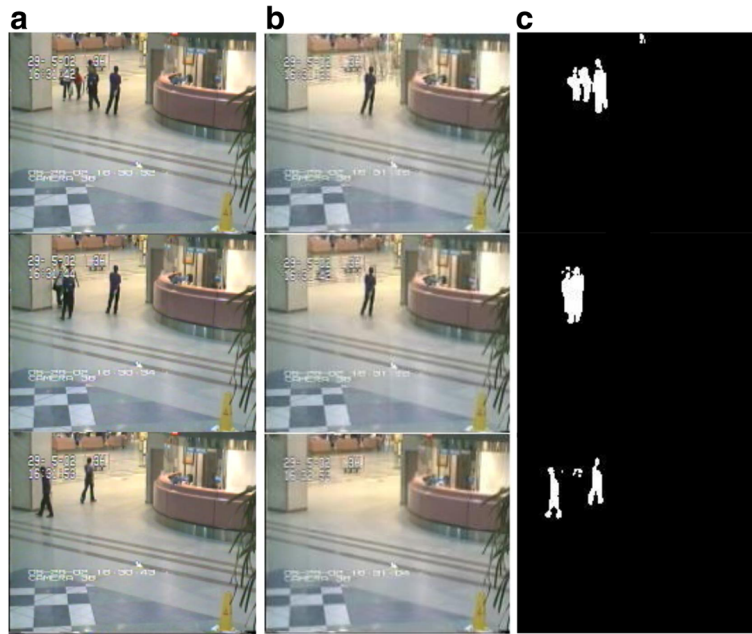


**Fig. 5** Background updating. **a** Image sequences with a stationary person. **b** The updated background. **c** The detection results

#### 4.1 Performance of the proposed approximative $\ell_1$ -min algorithm

In the first experiment, we compared the performance of solving the problem  $P_1$  or  $P_\lambda$  by eight  $\ell_1$ -min algorithms including gradient projection for sparse reconstruction (GPSR) [31], SPGL1-Lasso [32], orthogonal matching pursuit (OMP) [33], subspace pursuit (SP) [34], DGS [8], the Bregman iterative algorithm [15], l1-ls [35], and the proposed approximative  $\ell_1$ -min algorithm.

We randomly generated a one-dimensional (1D) sparse signal with values  $\pm 1$ , where the dimension  $n$  of the signal  $\alpha$  was 256. The observation matrix  $\mathbf{D}$  was generated by a  $m \times n$  matrix with independent and identically distributed (i.i.d.) elements derived from a Gaussian distribution  $N(0, 1)$ , and each row in the matrix was normalized to a unit magnitude. The recovery error and running time were introduced for quantitative evaluation. The recovery error is defined as the difference between the estimated signal  $\hat{\alpha}$  and the ground truth  $\alpha$ :  $\|\hat{\alpha} - \alpha\|_2 / \|\alpha\|_2$ . A comparison of the recovery error and running time performances of the eight  $\ell_1$ -min algorithms is shown in Fig. 6 with respect to a changing number of measurements  $m$ . To reduce the randomness, we repeat the experiment 100 times for each measurement number plotted in Fig. 6. With respect to the recovery error shown in Fig. 6a, the Bregman iterative algorithm [15] demonstrates the best performance while GPSR [31], SPGL1-Lasso [32], l1-ls [35], and the proposed method perform similarly and can be classified as the second performance tier. Relative to initial reports [8], the performance of DGS is sub-par because the simulated signal

has no distinct grouping trend. Fig. 6b shows that the proposed method consumes the least computation time of all methods considered regardless of the measurement number employed. The experimental results shown in Fig. 6 verify that the proposed approximative  $\ell_1$ -min algorithm can achieve competitive solutions with less complexity and reduced computational time for real-time BGS implementation.

To visually represent the performance of the eight  $\ell_1$ -min algorithms, we applied these algorithms to the two-dimensional (2D) Lena image  $\mathbf{I}$  ( $256 \times 256$ ), as shown in Fig. 7. The image was detached into non-overlapping  $8 \times 8$  patches. The dictionary  $\mathbf{D} \in \mathbb{R}^{64 \times 256}$  was pre-learned [29] with 256 atoms. The recovery error is defined as the difference between the recovery image  $\mathbf{D}\hat{\alpha}$  and the original image  $\mathbf{I}$ :  $\|\mathbf{D}\hat{\alpha} - \mathbf{I}\|_2 / \|\mathbf{I}\|_2$ . Figure 7a–h show the recovered Lena image (above) and the recovery error (below) by GPSR [31], SPGL1-Lasso [32], OMP [33], SP [34], DGS [8], the Bregman iterative algorithm [15], l1-ls [35], and the proposed approximative  $\ell_1$ -min algorithm, respectively. Although the recovered result is not the best, the proposed approach significantly accelerates the processing of the solution with least time, and as shown in Fig. 7, the difference between the results of the proposed method and those of the other methods is scarcely recognizable to the human eye, which indicates that the results of the proposed method are sufficiently accurate for the BGS problem. As described in Section 3.1, the numerical distance is tolerable for BGS, and the proposed  $\ell_1$ -min algorithm can be used to accelerate the proposed BGS method.

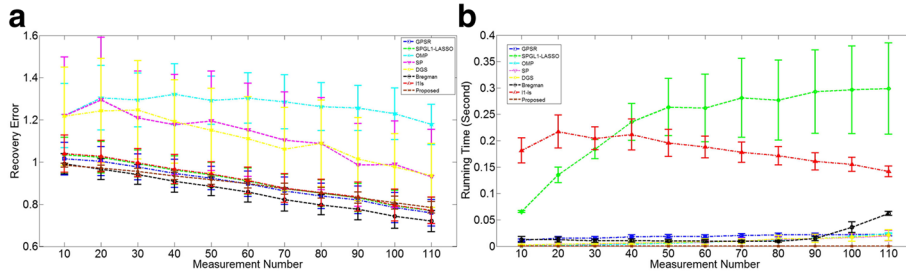


**Fig. 6** Recovery results with different measurement numbers. **a** The recovery error. **b** running time

**Algorithm 1:** Proposed BGS algorithm

**Input :** Image sequence  $I_1, I_2, \dots, I_M$ .

**Output:** The binary foreground  $I_1^F, I_2^F, \dots, I_M^F$ .

**Initialization:**

- 1 Compute the children sparse vector  $\beta$ .
- 2 Scale down the original sequence with a four to one ratio:  $I'_1, I'_2, \dots, I'_M$ .
- 3 Detach each frame  $I'_m$  into  $N$  non-overlapping patches:  $P_m^1, P_m^2, \dots, P_m^N$ .
- 4 Initialize the background model  $P_B^i = P_1^i \approx \mathbf{D} \times \sum_j \gamma_j^i \beta_j, i \in [1, \dots, N]$ .

**End initialization**

- 5 **for**  $m \leftarrow 2$  **to**  $M$  **do**
- 6     **for**  $i \leftarrow 1$  **to**  $N$  **do**
- 7         compute the foreground difference  $P_F^{mi}$  using Eq. (9);
- 8         detect the foreground region using Eqs. (10) and (11);
- 9         **if**  $P^{mi}$  is detected as a foreground region **then**
- 10             refine the corresponding region in  $I_m$  using Eq. (12);
- 11         **else**
- update background model  $P_B^{mi}$  using Eq. (13);

**4.2 Performance of the proposed BGS algorithm**

This section evaluates the performance of the proposed BGS method and is divided into two parts: qualitative and quantitative evaluation. All tested videos are  $160 \times 128$ . The dictionary sizes in the two-stage foreground detection are  $8 \times 8$  pixels with 256 atoms in the first stage and  $3 \times 3$  pixels with 256 atoms in the second stage. We qualitatively and quantitatively compare the proposed method with classic BGS algorithms including SOBS [5], ViBe [36], and SuBS [2], as well as the sparse and low-rank model of Xiao et al. [17], DECOLOR [22], MAMR [24], RePROCS [37], and GOSUS [27]. For all algorithms, we adjusted parameters to obtain what appeared to be optimal results on the tested dataset.

**4.2.1 Qualitative evaluation**

Movement in captured scenes can be divided into two parts. One part represents the foreground, which is an independent object that has no relationship to the scene. The other part is periodical or irregular, such as rain, snow, waves, and moving trees, and should be classified as the background based on its relevance to the scene. Therefore, an ability to distinguish the two types of movement becomes an important criterion for motion detection. In this section, we conduct experiments on real-image sequences from the I2R dataset [30] and CDnet dataset [38].

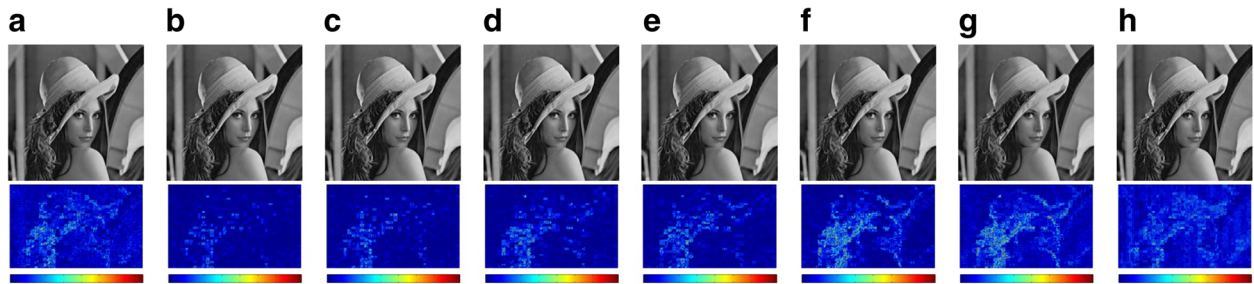


**Fig. 7** Comparison of recovered results with different  $\ell_1$ -min algorithms. The recovered Lena image (above) and the error (below) by **a** GPSR [31], **b** SPGL1-Lasso [32], **c** OMP [33], **d** SP [34], **e** DGS [8], **f** the Bregman iterative algorithm [15], **g** l1-ls [35], and **h** the proposed approximative  $\ell_1$ -min algorithm. The respective execution times of recovery are 180.9, 185.6, 10.3, 11.8, 12.0, 4.18, 163.9, and 0.08 s. The respective normalized errors of recovery at the pixel level are 0.0091, 0.0048, 0.0059, 0.0066, 0.0063, 0.0088, 0.0093, and 0.0204

We compared various motion detection approaches with the proposed method for the diverse dynamic scenes shown in Fig. 8a, where the ground truth BGS results are shown in Fig. 8b. The testing frames are extracted from the Curtain [30], Water Surface [30], Fountain [30], Fountain02 [38], Snow fall [38], and Skating [38] datasets, which include different types of periodical or irregular background motion such as a curtain blown by the wind, flowing water, or falling snowflakes. The first row contains a background subject to changes caused by the motion of a curtain, and the foreground consists of a moving person wearing a white shirt that is similar to the background. As shown in the top row of Fig. 8c, the proposed method detects the foreground well and is robust with respect to the curtain motion. The second row presents the same results with a fluctuating water surface.

SuBS [2] can handle the dynamic background well and generate robust detection results. Due to the post-process in SuBS, the results seem to be overly smooth. Similarly, DECOLOR [22] method has the same problem because the single regularized parameter cannot adequately distinguish the low-rank part (background) from the sparse error part (foreground). The Fountain and Fountain02 sequences present another form of non-stationary background. The results of SOBS [5] and the proposed method manage these conditions well. However, the floating water leads to false-positive results of Vibe [36], MAMR [24], and RePROCS [37]. Weather variations such as rain and

snow, which can be regarded as an irregular background motion, are also a challenge for BGS. The Snow fall and Skating datasets reflect this situation. However, the low-rank model GOSUS [27] cannot detect the left person in Skating due to the falling snow. The proposed method effectively eliminates the influence of the dynamic textures, and accurately detect the foreground. More discussion about the models comparison is shown in the following section.

#### 4.2.2 Quantitative evaluation

The quantitative performance of the algorithms is evaluated at the pixel level. Three different quantitative metrics, namely, Recall, Precision, and F-measure, were adopted. The three metrics are defined as follows [5].

$$\text{Recall} = \frac{tp}{tp + fn} \tag{14}$$

$$\text{Precision} = \frac{tp}{tp + fp} \tag{15}$$

$$\text{F-measure} = \frac{2 \times \text{RecallPrecision}}{\text{Recall} + \text{Precision}} \tag{16}$$

Here,  $tp$  is the number of pixels correctly classified as the foreground, whereas  $tp + fn$  and  $tp + fp$  are the number of pixels detected as foreground pixels by the ground truth and the proposed method, respectively. Therefore, Recall and Precision denote the percentage of detected true

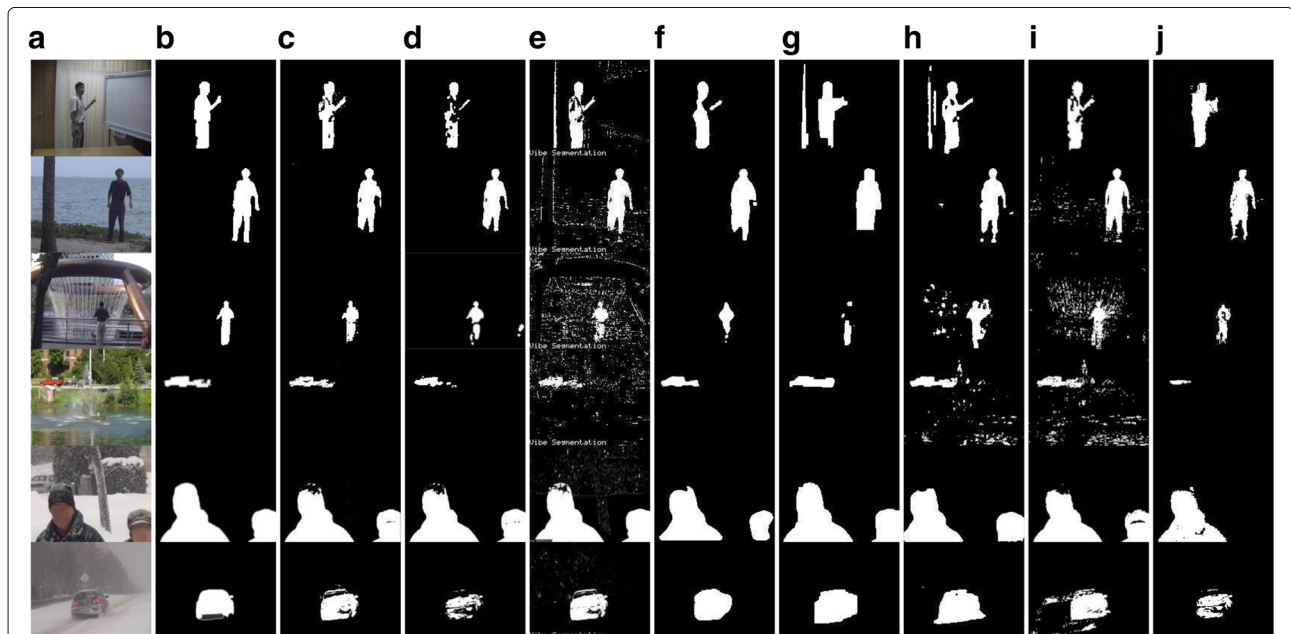


**Fig. 8** Comparison of detection results on dynamic videos. **a** The testing frames employed are extracted from datasets denoted as Curtain [30], Water Surface [30], Fountain [30], Fountain02 [38], Snow fall [38], and Skating [38] that present periodical or irregular background motion such as a curtain blown by the wind, flowing water, or falling snowflakes. **b** The ground truth BGS results. BGS detection results of **c** the proposed method, **d** SOBS [5], **e** Vibe [36], **f** SuBS [2], **g** DECOLOR [22], **h** MAMR [24], **i** RePROCS [37], and **j** GOSUS [27]

positives as compared to the total number of true positives in the ground truth and the total number of detected pixels in the proposed method. Because Recall and Precision conflict to each other, we employ the F-measure as the primary metric in the quantitative evaluation.

The CDnet [38] datasets are much larger and more abundant than any of the other datasets and include sufficient ground truth data for quantitative evaluation. Therefore, as listed in Table 1, we selected eighteen datasets from nine categories on the CDnet website, including baseline, dynamic background, intermittent object motion, shadow, thermal, bad weather, low frame rate, night videos, and turbulence. The quantitative results of the nine categories are listed in Table 1. We present the average frames per second by each method as shown in Table 2. In addition to the datasets employed in the above section, we present the results of 14 additional datasets obtained from CDnet [38] in Fig. 9. The third and sixth rows of Fig. 9 are the detection results of the proposed BGS method.

It is noted that the proposed BGS method obtained the best average *F-measure* compared to all other methods while SuBS [2] ranks second. Compared to the proposed method, SuBS [2] is sensitive to the Turbulence dataset due to the flow distortion. Besides, DECOLOR [22] has a good performance on F-measure while the frames per

second (fps) processed by DECOLOR [22] (MATLAB implementation) is only 2.3. The proposed method can achieve 29.3 fps while this number of MAMR (MATLAB implementation) is about 3.6. This accelerated processing speed is possible because the proposed method replaces an iterative optimization by linear addition and multiplication operations. For the baseline category (Office and PETS2006 datasets), the performances of all methods considered are acceptable. For the Fountain01 dataset, all the methods failed because the fountain movement exceeds the background updating capabilities of the methods. In contrast, the movement of Fountain02 is smooth and continuous, and SOBS [5] and SuBS [2] both perform well. The proposed method demonstrates competitive results for the thermal and turbulence categories (Park, dining room, turbulence0 and turbulence3 datasets). This is because the datasets of these two categories present distinct irregular fluctuations similar to noise that cannot be formulated by a mathematical expression. The proposed method employs sparsity over a pre-learned dictionary that can restrain this condition. The fps performance of low-rank methods such as RePROCS [37] and GOSUS is poor. This is because that the iterative pursuit of low-rank matrix or sparse matrix is time-consuming. The proposed approximative  $\ell_1$ -min algorithm avoids the iterative process and employs the power of sparse representation.

**Table 1** The quantitative F-measure metric (%) of the compared BGS methods on CDnet [38] datasets

Dataset	Classic methods			Low-rank methods				Sparse methods	
	SOBS	ViBe	SuBS	DECO	MAMR	GOSUS	RePROCS	Xiao	Proposed
Office	96.63	90.32	<b>97.02</b>	95.34	85.23	91.54	90.87	89.61	94.31
PETS2006	85.26	84.32	85.12	79.13	77.63	78.21	79.33	75.16	<b>86.16</b>
Fountain01	11.21	6.05	<b>15.63</b>	2.71	6.35	7.55	8.36	7.15	8.61
Fountain02	<b>85.81</b>	63.38	<i>84.69</i>	75.36	77.65	70.23	67.93	78.38	83.44
Parking	36.68	45.33	72.76	34.61	58.03	30.84	40.37	59.71	<b>75.31</b>
Sofa	62.18	61.97	62.69	50.31	63.46	51.24	47.87	<i>67.49</i>	<b>69.63</b>
Cubicle	72.05	<b>79.65</b>	79.33	77.67	69.38	71.23	69.34	70.91	73.64
Copy Machine	57.21	<i>81.71</i>	<b>89.74</b>	78.18	70.68	79.22	74.32	69.61	75.61
Park	59.70	69.53	58.69	<b>75.81</b>	70.96	72.33	66.98	70.14	74.73
Dining Room	71.73	75.49	70.36	<i>82.47</i>	78.33	76.48	70.38	72.30	<b>84.67</b>
Snow fall	67.01	82.49	<i>85.03</i>	83.46	82.36	81.84	76.70	73.41	<b>85.27</b>
Skating	76.33	73.67	80.25	83.81	85.68	79.83	75.93	78.64	82.11
Tram Crossroad	74.18	<b>85.64</b>	71.36	74.62	76.69	75.65	67.33	71.49	75.29
Turnpike	78.98	<b>90.64</b>	<i>89.67</i>	88.37	85.44	85.45	79.43	79.61	86.82
Winter Street	51.04	30.58	55.56	<b>66.13</b>	49.64	38.45	33.20	57.91	<i>60.34</i>
Tram Station	71.32	70.69	72.91	69.54	70.03	72.98	68.26	61.41	<b>76.17</b>
Turbulence0	2.64	5.36	8.65	<i>38.34</i>	35.67	37.94	33.62	29.34	<b>40.34</b>
Turbulence3	74.96	65.48	80.28	77.67	<i>81.36</i>	68.29	59.33	79.56	<b>87.64</b>
Average	63.05	64.57	<i>69.98</i>	68.53	68.03	64.96	61.64	66.21	<b>73.33</b>

Best, bold; second best, italics

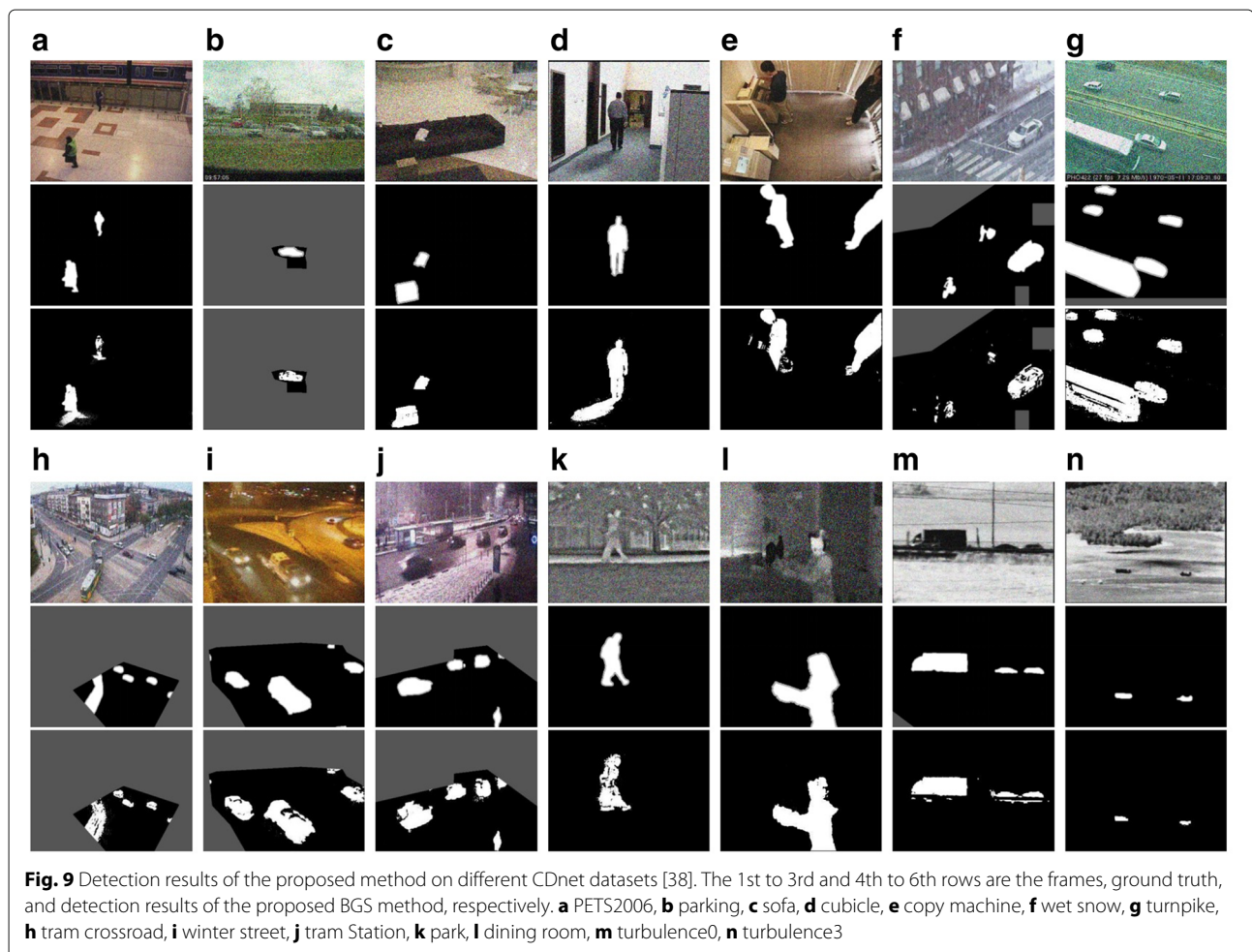
**Table 2** Average frames per second (FPS) of each method

Dataset	Classic methods			Low-rank methods				Sparse methods	
	SOBS	ViBe	SuBS	DECO	MAMR	GOSUS	RePROCS	Xiao	Proposed
FPS	28.5	31.9	48.7	2.3	3.6	0.54	0.78	2.6	29.3
Platform	C++	C++	C++	MATLAB	MATLAB	MATLAB	MATLAB	MATLAB	MATLAB

### 5 Conclusions

Sparse and low-rank model based BGS applications and methods have received considerable attention. However, the iterative optimization process used to obtain sparse or low-rank solutions is computationally expensive. This paper proposed the approximative  $\ell_1$ -min algorithm to provide a level of computational efficiency unobtainable by previous sparse model based approaches. Moreover, the proposed approach employed the sparsity rather than the sparse error to detect the foreground, which has been proven effective and robust to dynamic and corrupted scenes.

However, this work is at a preliminary stage. For example, how the signal should be separated into basic atoms  $e_i$  remains an open question, even though a satisfactory result can be obtained in separating the signal using the simplest method, as demonstrated in Eq. (3) by this work. Another future work is to measure the numerical differences of the sparse solution between the proposed  $\ell_1$ -min method and existing  $\ell_1$ -min algorithms. The difference is acceptable for motion detection, but this does not ensure it can be used for other applications. Thus, mathematically defining this difference is required to determine the potential of the proposed algorithm.



### Acknowledgements

This research was partially supported by National Natural Science Foundation (NSFC) of China under project No. 61403403 and No. 61402491.

### Authors' contributions

HX carried out the main part of this manuscript. YL participated in the design of the approximative  $\ell_1$ -min algorithm. MZ participated in the discussion. All authors read and approved the final manuscript.

### Competing interests

The authors declare that they have no competing interests.

Received: 29 June 2016 Accepted: 30 November 2016

Published online: 12 December 2016

### References

1. T Bouwmans, Traditional and recent approaches in background modeling for foreground detection: An overview. *Comput. Sci. Rev.* **11**, 31–66 (2014)
2. P St-Charles, G Bilodeau, R Bergevin, Subsense: a universal change detection method with local adaptive sensitivity. *IEEE Trans. Image Process.* **24**(1), 359–373 (2015)
3. C Stauffer, WEL Grimson, in *Proceedings of the IEEE Comput. Vis. Pattern Recognit. (CVPR)*. Adaptive background mixture models for real-time tracking (IEEE, Ft. Collins, 1999), pp. 246–252
4. NM Oliver, B Rosario, AP Pentland, A Bayesian computer vision system for modeling human interactions. *IEEE Trans. Pattern Anal. Mach. Intell.* **22**(8), 831–843 (2000)
5. L Maddalena, A Petrosino, A self-organizing approach to background subtraction for visual surveillance applications. *IEEE Trans. Image Process.* **17**(7), 1168–1177 (2008)
6. YC Eldar, G Kutyniok (eds.), *Compressed Sensing: Theory and Applications* (Cambridge University Press, Cambridge CB2 8RU, 2012)
7. V Cevher, A Sankaranarayanan, MF Duarte, D Reddy, RG Baraniuk, R Chellappa, in *Proceedings of the European Conf. Comput. Vis. (ECCV)*. Compressive sensing for background subtraction (Springer, Marseille, 2008), pp. 155–168
8. J Huang, X Huang, D Metaxas, in *Proceedings of the IEEE Int. Conf. Comput. Vis. (ICCV)*. Learning with dynamic group sparsity (IEEE, Kyoto, 2009), pp. 64–71
9. R Sivalingam, D Alden, B Michael, M Roland, V Morellas, N Papanikolopoulos, in *Proceedings of the IEEE Int. Conf. Rob. Autom. (ICRA)*. Dictionary learning for robust background modeling (IEEE, Shanghai, 2011), pp. 4234–4239
10. C Zao, X Wang, W-K Cham, Background subtraction via robust dictionary learning. *EURASIP J. Image Video Process.* 1–12 (2011)
11. M Osborne, B Presnell, B Turlanch, A new approach to variable selection in least squares problems. *IMA J. Numer. Anal.* **20**(3), 389–404 (2000)
12. B Efron, T Hastie, I Johnstone, R Tibshirani, Least angle regression. *Ann. Stat.* **32**(2), 407–499 (2004)
13. J Friedman, T Hastie, R Tibshirani, Pathwise coordinate optimization. *Ann. Appl. Stat.* **1**(2), 302–332 (2007)
14. E Hale, W Yin, Y Zhang, A fixed-point continuation method for  $\ell_1$  regularized minimization with applications to compressed sensing. *CAAM TR07-07*, Rice University. **43**, 1–44 (2007)
15. W Yin, S Osher, D Goldfarb, J Darbon, Bregman iterative algorithms for compressed sensing and related problems. *SIMA J. Imag. Sci.* **1**(1), 143–168 (2008)
16. G Xue, L Song, J Sun, Foreground estimation based on linear regression model with fused sparsity on outliers. *IEEE Trans. Circ. Syst. Video Technol.* **23**(8), 1346–1357 (2014)
17. H Xiao, Y Liu, S Tan, J Duan, M Zhang, A noisy videos background subtraction algorithm based on dictionary learning. *KSII Trans. Internet Inf. Syst.* **8**(6), 1946–1963 (2014)
18. T Bouwmans, E Zahzah, Robust PCA via principal component pursuit: a review for a comparative evaluation in video surveillance. *Comp. Vision Image Underst.* **122**, 22–34 (2014)
19. C Qiu, N Vaswani, in *Proceedings of the IEEE Communication, Control, and Computing*. Real-time robust principal components' pursuit (IEEE, Tamil Nadu, 2010), pp. 591–598
20. E Candès, X Li, Y Ma, J Wright, Robust principal component analysis? *J. ACM.* **58**(3), 1–37 (2011)
21. X Cui, J Huang, S Zhang, D Metaxas, in *Proceedings of the European Conf. Comput. Vis. (ECCV)*. Background subtraction using low rank and group sparsity constraints (Springer, Firenze, 2012), pp. 612–625
22. X Zhou, C Yang, W Yu, Moving object detection by detecting contiguous outliers in the low-rank representation. *IEEE Trans. Pattern Anal. Mach. Intell.* **35**(3), 597–610 (2013)
23. P Rodríguez, B Wohlberg, in *Proceedings of the IEEE Image Processing. A Matlab implementation of a fast incremental principal component pursuit algorithm for video background modeling* (IEEE, Paris, 2014), pp. 3414–3416
24. X Ye, J Yang, X Sun, K Li, C Hou, Y Wang, Foreground-background separation from video clips via motion-assisted matrix restoration. *IEEE Trans. Circ. Syst. Video Technol.* **25**(11), 1721–1734 (2015)
25. J He, L Balzano, A Szlam, in *Proceedings of the IEEE Comput. Vis. Pattern Recognit. (CVPR)*. Incremental gradient on the Grassmannian for online foreground and background separation in subsampled video (IEEE, Boston, 2012), pp. 1568–1575
26. F Seidel, C Hage, M Kleinsteuber, pROST—a smoothed Lp-norm robust online subspace tracking method for realtime background subtraction in video. *Mach. Vis. Appl.* **122**, 1–13 (2013)
27. J Xu, V Ithapu, L Mukherjee, JM Rehg, V Singh, in *Proceedings of the IEEE Int. Conf. Comput. Vis. (ICCV)*. Gosus: Grassmannian online subspace updates with structured-sparsity (IEEE, Sydney, 2013), pp. 3376–3383
28. D Donoho, X Huo, Uncertainty principles and ideal atomic decomposition. *IEEE Trans. Inf. Theory.* **47**(7), 2845–2862 (2001)
29. J Mairal, F Bach, J Ponce, G Sapiro, Online learning for matrix factorization and sparse coding. *J. Mach. Learn. Res.* **11**, 19–60 (2010)
30. L Li, W Huang, IYH Gu, Q Tian, Statistical modeling of complex backgrounds for foreground object detection. *IEEE Trans. Image Process.* **13**(11), 1459–1472 (2004)
31. M Figueiredo, R Nowak, S Wright, Gradient projection for sparse reconstruction: application to compressed sensing and other inverse problems. *IEEE J. Sel. Top. Sign. Process.* **1**(4), 586–597 (2007)
32. E Berg, M Friedlander, Sparse optimization with least-squares constraints. *SIAM J. Optim.* **21**(4), 1201–1229 (2011)
33. J Tropp, A Gilbert, Signal recovery from random measurements via orthogonal matching pursuit. *IEEE Trans. Inf. Theory.* **53**(12), 4655–4666 (2007)
34. D Wei, M Olgica, Subspace pursuit for compressed sensing signal reconstruction. *IEEE Trans. Inf. Theory.* **55**(5), 2230–2249 (2009)
35. S-J Kim, K Koh, M Lustig, S Boyd, D Gorinevsky, An interior-point method for large-scale  $\ell_1$ -regularized least square. *IEEE J. Sel. Top. Sign. Process.* **1**(4), 606–617 (2007)
36. O Barnich, MV Droogenbroeck, Vibe: A universal background subtraction algorithm for video sequences. *IEEE Trans. Image Process.* **20**(6), 1709–1724 (2011)
37. H Guo, N Vaswani, C Qiu, in *Proceedings of IEEE Global Signal and Information Processing*. Practical ReProcs for separating sparse and low-dimensional signal sequences from their sum—part 2 (IEEE, Atlanta, 2014), pp. 369–373
38. N Goyette, P Jodoin, F Porikli, J Konrad, P Ishwar, in *Proceedings of the IEEE Comput. Vis. Pattern Recognit. Workshops (CVPRW)*. Changedetection.net: a new change detection benchmark dataset (IEEE, Boston, 2012), pp. 1–8